Science Advances
AAAS

advances.sciencemag.org/cgi/content/full/6/40/eabb9062/DC1

Supplementary Materials for

Thermofluidic heat exchangers for actuation of transcription in artificial tissues

Daniel C. Corbett, Wesley B. Fabyan, Bagrat Grigoryan, Colleen E. O'Connor, Fredrik Johansson, Ivan Batalov, Mary C. Regier, Cole A. DeForest, Jordan S. Miller, Kelly R. Stevens*

*Corresponding author. Email: ksteve@uw.edu

Published 30 September 2020, *Sci. Adv.* **6**, eabb9062 (2020)
DOI: 10.1126/sciadv.abb9062

The PDF file includes:

Figs. S1 to S10

Other Supplementary Material for this manuscript includes the following:

(available at advances.sciencemag.org/cgi/content/full/6/40/eabb9062/DC1)

Movie S1

Supplemental Figures:

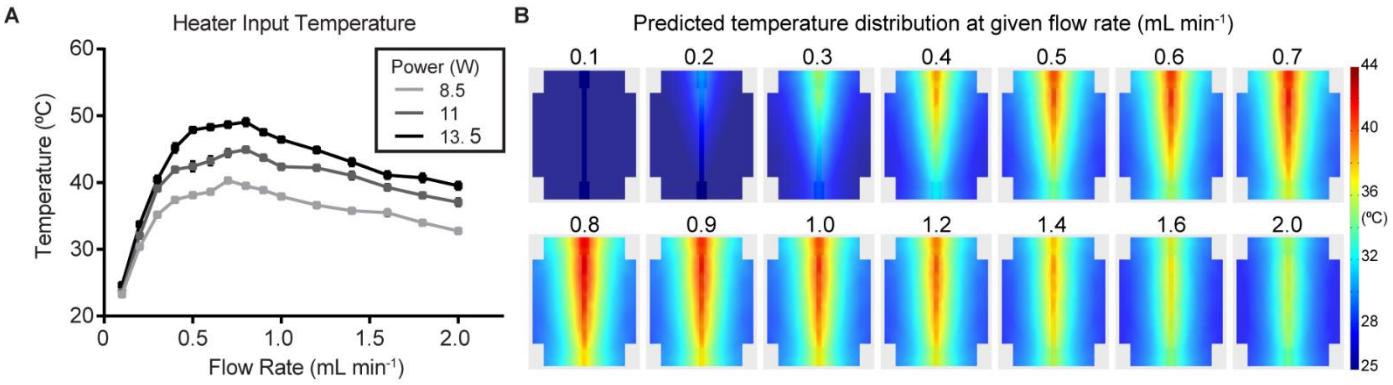

Figure S1 | Computational modeling of flow rate in fluidic hydrogel heating system

A, Measurements of fluid temperature at heater outflow indicate that both fluid flow rate and heating element power affect hydrogel inlet temperature (n = 3, data represent mean temperature ± standard error). **B**, Full dataset of finite element modeling predictions of temperature distribution in perfused hydrogels at flow rate and temperature combinations from the 13.5 W curve in A. Hyperthermic temperatures are predicted at the hydrogel surface with perfusion flow rates ranging 0.4 – 1.6 mL min^{-1}.

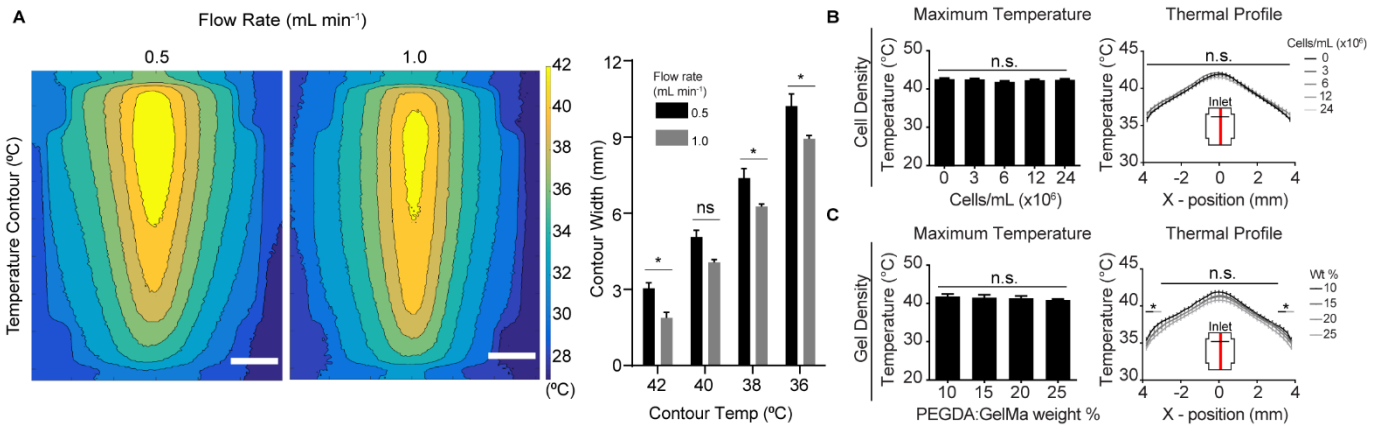

Figure S2 | Spatial temperature analysis for hydrogel perfusion flow rate, weight percentage, and cell density. **A**, Representative isothermal contour plots generated from infrared images in Fig 2D (left, scale bars = 5 mm). Measurements of contour width along the width (x) at the inlet (right) show that contour width is significantly greater for flow at 0.5 mL min^{-1} compared to 1.0 mL min^{-1} for 42 ºC, 38 ºC and 36 ºC contours (n = 5, error bars represent standard error, *p<0.05 by two-way ANOVA followed by Sidak's multiple comparison test). **B**, Thermal quantification of thermofluidic gels with varying cell density (0 - 24 x 10^6 cells mL^{-1}). No significant changes in peak temperature (left) were recorded for any cell density condition (n = 6, data are mean temperature ± standard error, non-significant, n.s, one-way ANOVA followed by Tukey's multiple comparison test). Thermal profiles (right) measured at the inlet position across hydrogel width (x) overlay each other for all cell density conditions (n = 6, data are mean temperature ± standard error, non-significant, n.s, two-way ANOVA followed by Tukey's multiple comparison test). **C**, Thermal quantification of thermofluidic gels with varying gel density (10 - 25 %, 50:50 6K PEGDA:GelMa weight %). Peak temperatures did not change across hydrogel weight % conditions (n = 6, data are mean temperature ± standard error, non-significant, n.s, one-way ANOVA followed by Tukey's multiple comparison test). Thermal profiles (right) showed significant decreases in temperature at the gel periphery in 25 wt% gels compared to 10 wt% gels (n = 6, data are mean temperatures ± standard error, non-significant, n.s., *p<0.05 by two-way ANOVA followed by Tukey's multiple comparison test).

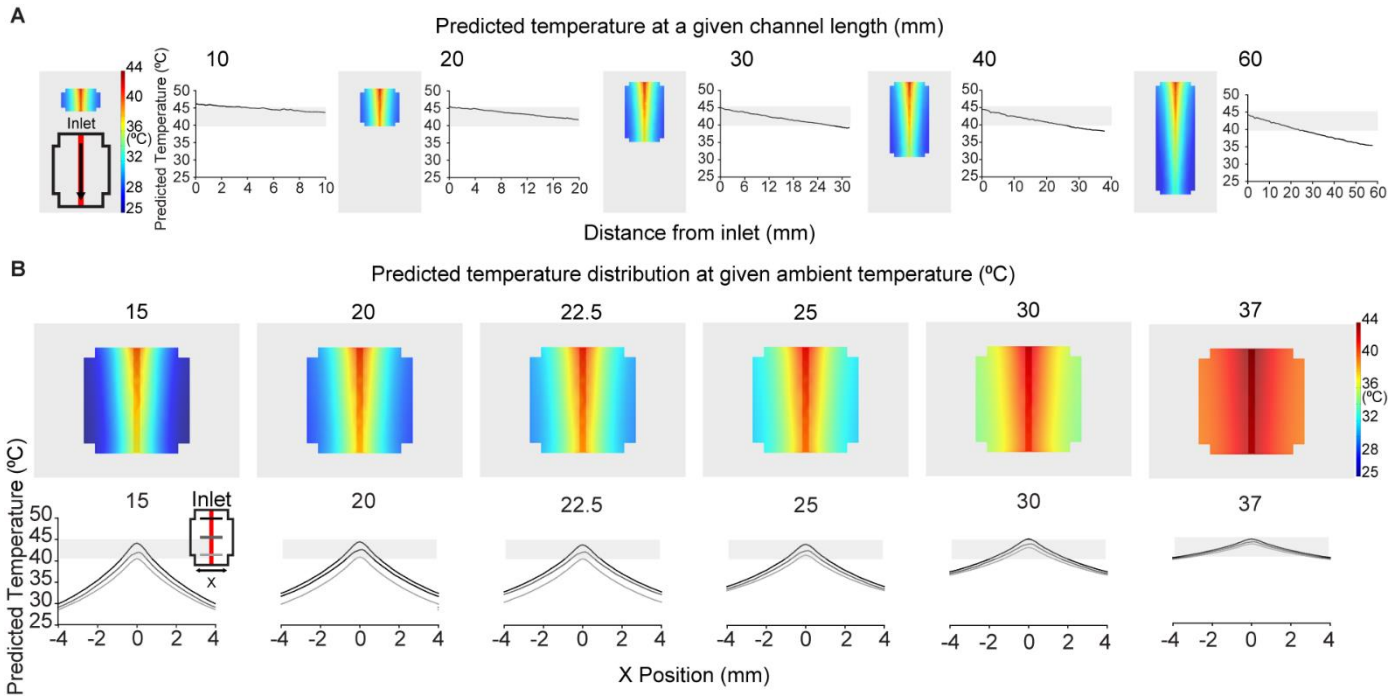

Figure S3 | Computational characterization of thermofluidic dimensions and ambient conditions

A, Finite element modeling predictions of temperature distribution in perfused gels of varying channel length predict that hydrogels up to 30 mm long achieve hyperthermic temperature ranges along their full length (hyperthermic region (40 – 45 ºC), gray shading). **B**, Finite element modeling predictions of temperature distribution in perfused gels at varying ambient temperature.

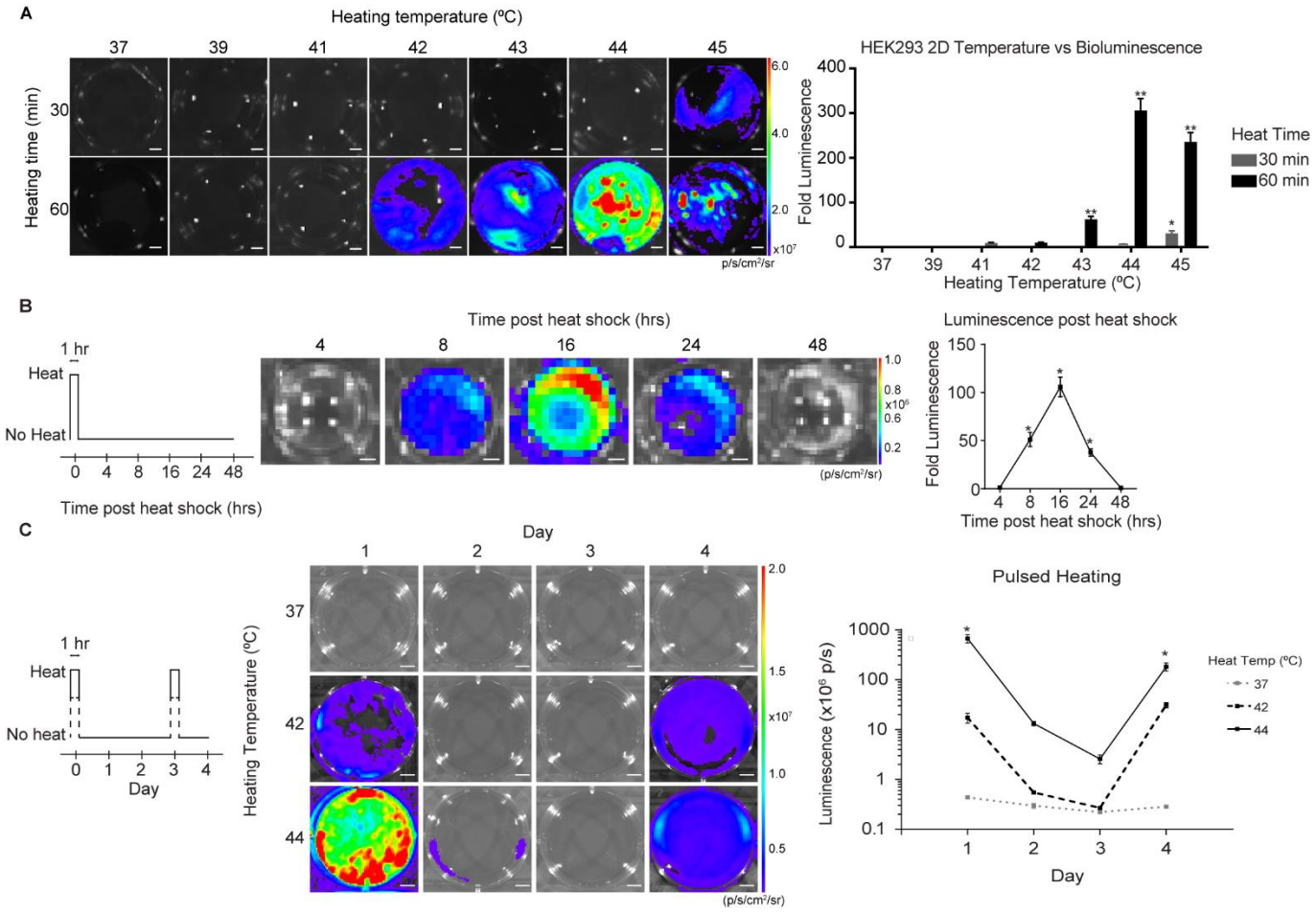

Figure S4 | Heat treatment upregulates reporter genes in 2D cultured cells. A, HEK293T cells transduced with human heat shock promoter 6a driving firefly luciferase exhibit a temperature dose-dependent upregulation of luciferase in 2D culture, as shown in representative luminescent images of differentially heated culture wells (left) and quantification of fold change in luminescence over 37ºC control (right, scale bars = 5 mm; n=3, data are mean fold luminescence ± standard error, *p < 0.05, **p < 0.01 by two-way ANOVA followed by Dunnett's multiple comparisons test). **B**, Heat inducible HEK293T cells were heat shocked for 1 hour at 44ºC and luminescence was quantified at various time points between 4 and 48 hours after heat shock induction showing significant signal compared t between 8 - 24 hours and peaking at 16 hours (scale bars = 1 mm; n = 9, data are mean fold luminescence ± standard error, *p<0.05 by one-way ANOVA followed by Dunnett's multiple comparison test). **C**, Heat inducible HEK293T cells were heat shocked twice, at 42ºC or 44ºC, over the course of four days at days 0 and 3 with luminescence

measured each day. Significant increases in luminescence were observed at 44ºC compared to 37ºC controls at days 1 and 4 (scale bars = 5 mm; n = 6, data are mean luminescence error bars ± standard error, *p<0.05 by two-way ANOVA followed by Tukey's multiple comparison test).

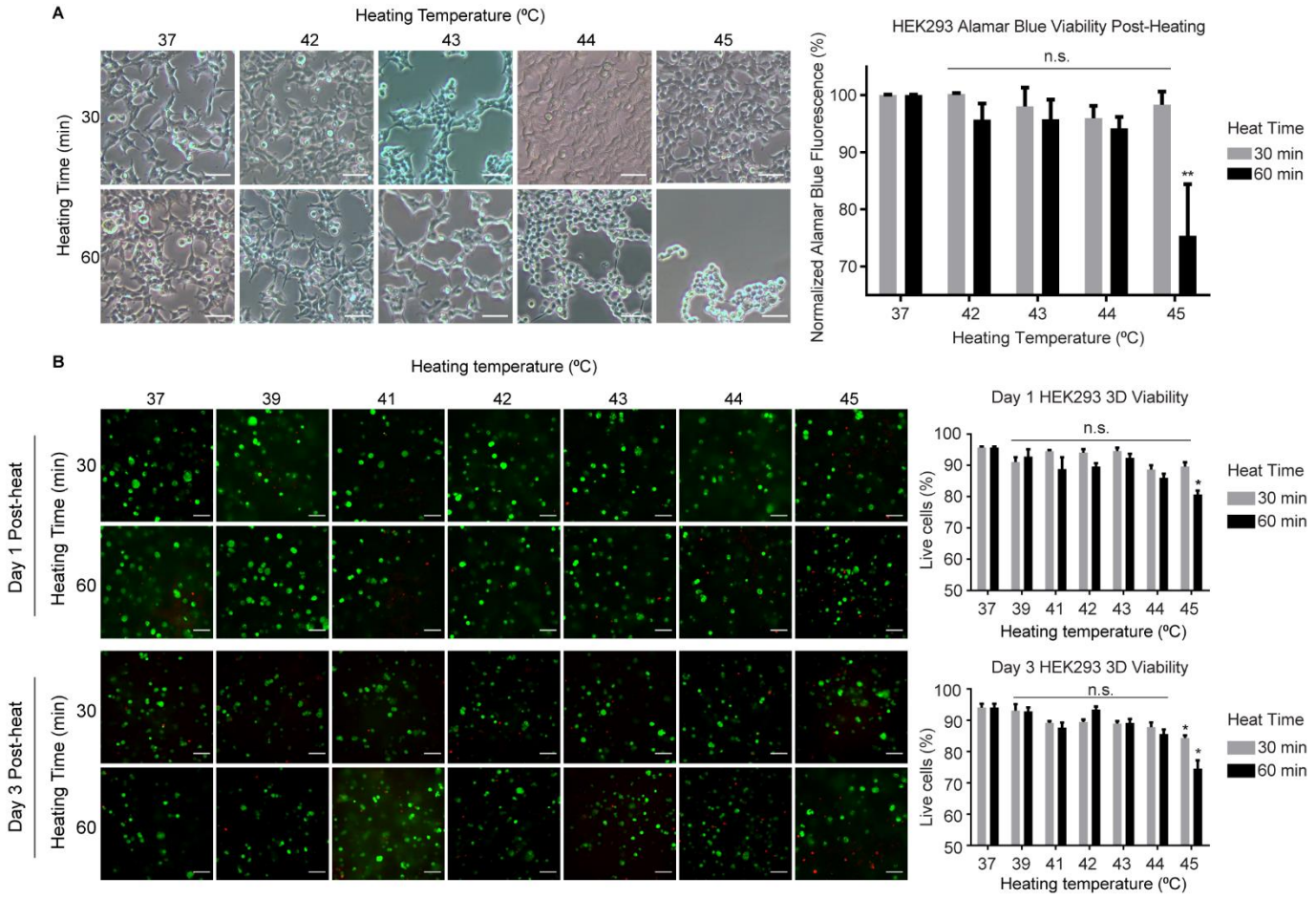

Figure S5 | Characterization of thermal dosage effect on cell viability in 2D and 3D. **A**, HEK293T cells cultured on tissue culture plastic demonstrated typical morphology upon exposure to 37-43ºC, became rounded upon exposure to 44ºC, and began to detach upon exposure to 45ºC after 60 minutes (left, scale bars = 50 µm). A significant decrease in cell reducing potential was observed after 60 min of heating at 45ºC but not at other temperatures (Alamar blue assay; fluorescence normalized to 37ºC condition; n = 3, data are mean fluorescence percentage ± standard error, non-significant, n.s., **p < 0.01 by two-way ANOVA followed by Dunnett's multiple comparisons test. **B**, HEK293T cells printed in 3D hydrogels and

exposed to the same hyperthermic conditions as in A show a similar viability trend as shown in representative Calcein/Ethidium Homodimer (Live/Dead) staining images. A signficant decrease in viability is seen in hydrogels exposed to 45ºC for 60 minutes at 1 and 3 days post-heating and at 45ºC for 30 minutes 3 days post-heating but not at other temperature-time conditions (n=5, data are mean percentage ± standard error, non-significant, n.s., *p<0.05 by two-way ANOVA followed by Dunnett's multiple comparisons test).

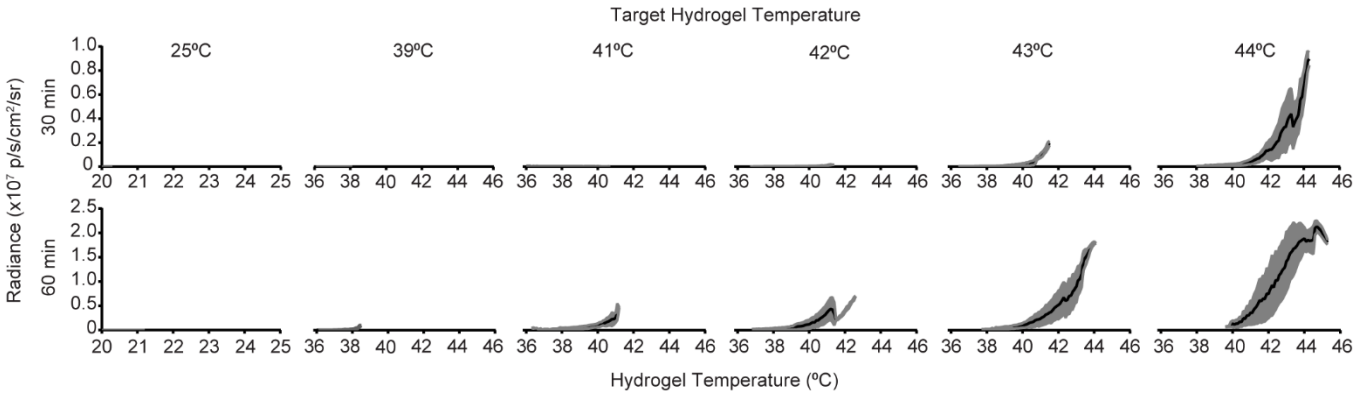

Figure S6 | Temperature expression relationship in differentially heated hydrogels. Response curves from each hydrogel temperature condition. Data points from these plots were combined to make Fig 3J. Analysis shows in 60 min heating charts, bioluminescence is activated beginning at 40ºC, increases non-linearly and peaks at ~44ºC. Above 44ºC bioluminescence begins to drop off due to thermal stress (Fig S5). Data are mean radiance (black curve) ± standard deviation (shaded area).

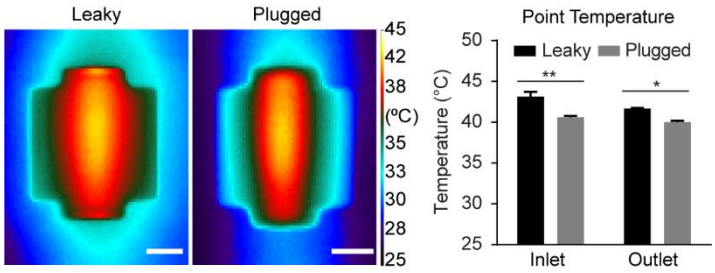

Figure S7 | Optimization of perfusion apparatus and connectivity improves thermal patterning. Improper fitting between printed hydrogels and perfusion chips can result in slight leakages that lead to accumulation of heated fluid which subsequently raise local temperature at inlet and outlet positions. Optimization of connectivity between the heating apparatus tubing and hydrogel channel networks with a custom-designed perfusion chip addresses this challenge (scale bars = 2 mm; n = 3, data are mean temperatures ± standard error, *p<0.05, **p<0.01 by two-way ANOVA followed by Sidak's multiple comparison test).

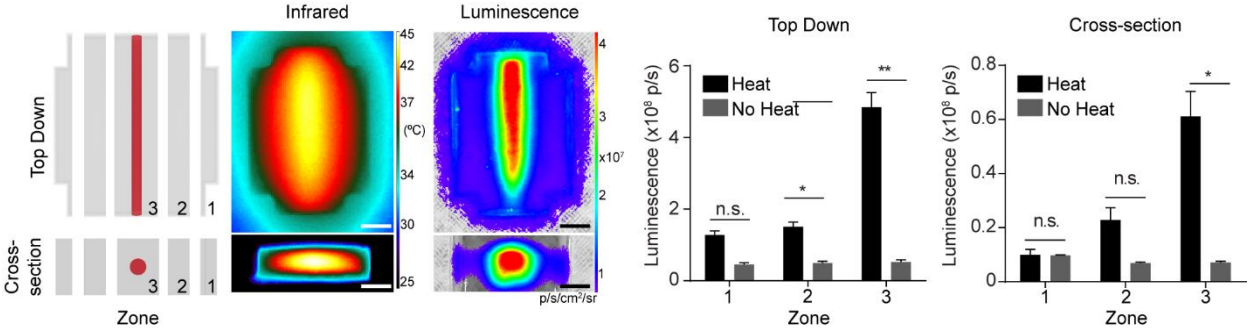

Figure S8 | Multi-perspective bioluminescent imaging of thermofluidically heated gels. Bioluminescence from single channel heated gels was quantified by dividing each gel into 3 zones and viewing the gels from 'Top-down' and 'Cross-section' perspectives (scale bars = 2 mm). Luminescence quantification under both perspectives shows peak expression occurs nearest the channel and decays radially outwards (n=5, data are mean luminescence ± standard error, non-significant, n.s., *p<0.05, **p<0.01 by two-way ANOVA followed by Sidak's multiple comparisons test).

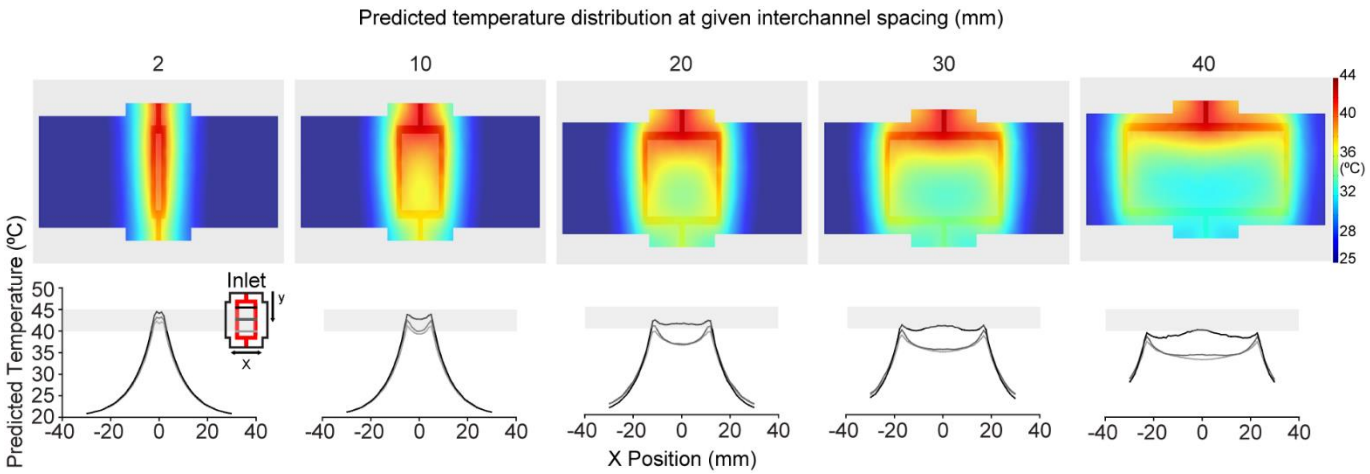

Figure S9 | Finite element modeling predictions of temperature distribution in perfused branched channel gels at varying interchannel spacing. Bifurcating channel geometries with daughter branches spaced at interchannel distances from 2 – 40 mm were computationally modeled (top). Hyperthermic temperature ranges are predicted across hydrogel width (x) between the channels at inlet (black), middle (dark grey) and outlet (light grey) positions for 2 – 10 mm interchannel spacings (bottom).

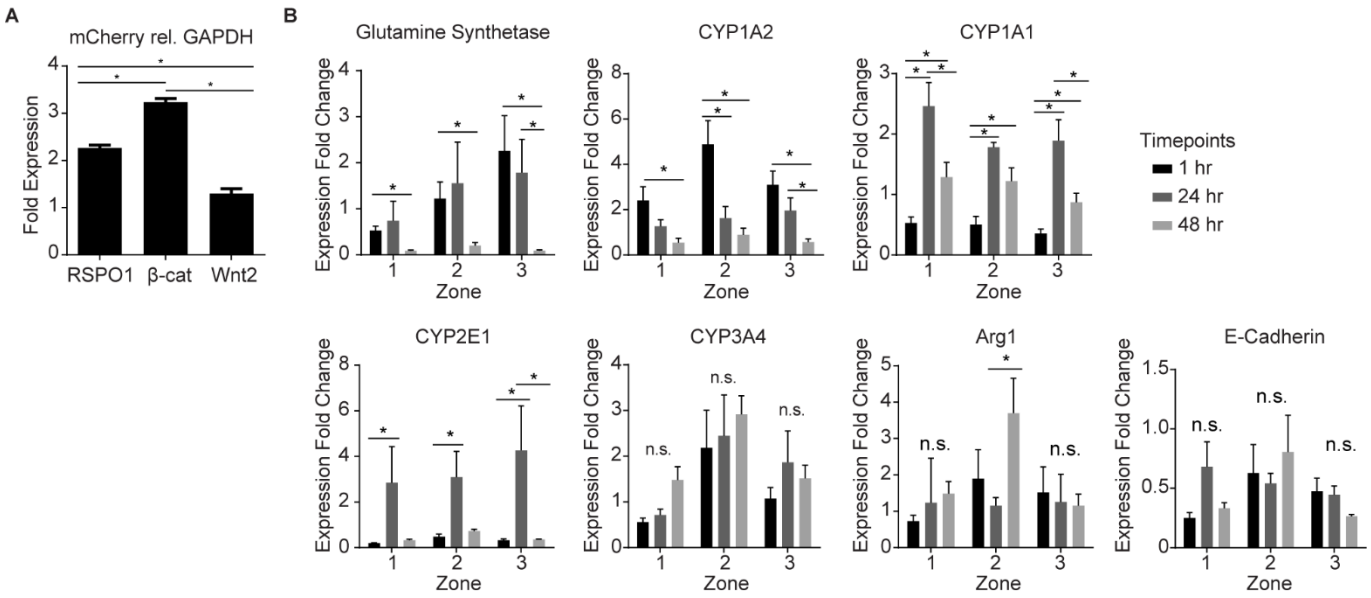

Figure S10 | Expression variation and zonal regulation of pericentral/periportal gene markers in HEAT activated HEK293T and HepaRG cells. **A**, Variations in mCherry expression are observed between individual heat-inducible HEK293T cells indicating different levels of promoter integration (n = 3, data are mean fold ± standard error, *p<0.05 by one-way ANOVA followed by Tukey's multiple comparison test). **B**, Zonal expression profiles for pericentral (Glutamine Synthetase, CYP1A2, CYP1A1, CYP2E1, CYP3A4) and periportal/midzonal (E-Cadherin, Arg1) genes assayed in heat-induced RSPO1 HepaRG at different times post heating. Temporal upregulation of canonical pericentral Wnt responsive genes (Glutamine Synthetase, CYP1A2) is seen at 1 and 24 hours and CYP2E1 at 24 hours in comparison to 48 hours after for Zones 1, 2, and 3. Trending spatial zonation patterns (increase in expression from Zone 1 to Zone 3) are seen for Glutamine Synthetase and CYP2E1, but these were not statistically significant. Periportal/midzonal gene Arg1 shows significant upregulation in Zone 2 for the 48 hour timepoint in comparison to the 1 hour and 24 hour timepoint, while periportal E-cadherin shows no zonal differences (n = 15 - 30, data are mean fold change ± standard error, *p<0.05 by two-way ANOVA followed by Tukey's multiple comparison test).